SHORT COMMUNICATION OPEN ACCESS

Molecular Immunology and Signaling

CST Is Epistatic With Shieldin to Limit DNA Double-Strand Break End Resection and Promote Repair During *Igh* Class Switch Recombination

Chloé Lescale[1] 🔵 | Timea Marton[1] 🔵 | Amaury Vaysse[1,2] 🔵 | Guillaume Rode[1] 🔵 | Estelle Vincendeau[1] 🔵 |
Alice Libri[1] 🔵 | François Dossin[1] 🔵 | Ludovic Deriano[1] 🔵

[1]Institut Pasteur, Université Paris Cité, INSERM U1223, Genome Integrity Immunity and Cancer Unit, Équipe Labellisée Ligue Contre Le Cancer, Paris, France |
[2]Institut Pasteur, Université Paris Cité, Bioinformatics and Biostatistics Hub, Paris, France

Correspondence: Chloé Lescale (chloe.lescale@pasteur.fr) | Ludovic Deriano (ludovic.deriano@pasteur.fr)

ABSTRACT

Downstream of 53BP1-RIF1 lies the Shieldin (SHLD) protein complex, which comprises MAD2L2/REV7, SHLD3, SHLD2, and SHLD1, and the CTC1-STN1-TEN1 (CST) complex. During immunoglobulin heavy-chain (*Igh*) class switch recombination (CSR), 53BP1-RIF1-SHLD promotes productive end-joining by limiting resection of activation-induced cytidine deaminase (AID)-generated DNA double-strand break (DSB) ends. The precise role of the CST complex and its interplay with SHLD during CSR is however elusive. Here, we established AID-inducible B cell lines deficient for CTC1, SHLD1, or both and analyzed CSR in these cells. We show that stimulated CTC1-deficient B cells are defective for IgM-to-IgA class switching, accumulate *Igh* chromosome breaks and translocations, and display increased end-resection and micro-homology usage at switching sites, demonstrating that CTC1 is essential to suppress alternative end-joining during CSR. We show that CTC1 and SHLD1 are epistatic in preventing exacerbated DNA end resection and genetic instability during CSR. Moreover, using a complementation approach in *Shld1* knockout splenic B cells, we show that a SHLD1 mutant defective in CST binding (SHLD1^ΔLDLP) is fully proficient for IgM-to-IgG1, IgG2b, IgG3, and IgA class switching, thus demonstrating that the SHLD1-CTC1 interaction through this motif is dispensable for CST and SHLD functions in promoting CSR.

1 | Introduction

DNA double-strand breaks (DSBs) are common cytotoxic lesions that continually threaten genome integrity. DSBs can be repaired by multiple pathways, the choice of which depends largely on the structure of the DNA ends and the propensity of the cell to engage DSB end resection. Two programmed recombination mechanisms participate in the generation of antigen receptor diversity in adaptive immune cells—V(D)J recombination that occurs in developing B and T lymphocytes, and class switch recombination (CSR) that takes place in mature B cells [1, 2]. CSR modifies antibody effector functions by replacing the isotype expressed from IgM/IgD to IgG, IgA, or IgE. At the DNA level, this is achieved by a deletional recombination event at the *Igh* locus between a donor (Sμ) and an acceptor repetitive switch region (Sx) that brings into proximity the V region and the exons encoding a new constant region thus allowing the expression of an antibody with a different isotype but with the same specificity

[2]. S regions consist of highly repetitive 1–12-kilobase sequences with G-rich nontemplate strands [2, 3]. During CSR, activation-induced cytidine deaminase (AID) deaminates cytosines into uracils in transcribed S-regions, which are converted to DSBs with the help of base excision and mismatch repair proteins. CSR is completed by fusing donor and acceptor S-region DSB ends by NHEJ and, in its absence, by alternative end-joining (alt-EJ) that is more biased to use longer junctional microhomologies (MHs) [4, 5]. AID-induced DNA breaks are thought to be composed of a mixture of blunt and single-stranded (ss) DSB ends, which necessitate protection against resection by the chromatin-bound protein 53BP1 and its multiple downstream effectors [6].

Mechanistically, 53BP1 recruits RIF1 to shield DSB ends against resection, thereby favoring repair by NHEJ over homology-dependent repair pathways such as homologous recombination (HR), single-strand annealing (SSA) or alt-EJ [4, 6]. Acting downstream of 53BP1-RIF1 is the Shieldin (SHLD) protein complex, comprised of REV7/MAD2L2, SHLD1, SHLD2, and SHLD3, and the CTC1-STN1-TEN1 (CST) complex [6–8]. The precise mechanisms through which 53BP1-RIF1-SHLD-CST inhibits DSB end resection remain unclear. Two models have been proposed: protection against the action of exonucleases by SHLD and CST, and localized fill-in DNA synthesis by CST and DNA polymerase α (Polα)-primase [7–11]. The recruitment of SHLD to DSBs is mediated by the association of SHLD3 to 53BP1-RIF1. SHLD3 also interacts with REV7 which bridges SHLD2 and SHLD1. SHLD2 interacts with ssDNA through its C-terminal oligonucleotide/oligosaccharide-binding (OB) fold region, which is essential for the ability of the complex to repress resection. CST also forms an ssDNA binding complex containing OB-fold domains, which may, in turn, inhibit resection. Epistasis between 53BP1-RIF1, SHLD, and CST is evident in multiple NHEJ reactions, including CSR, the fusion of telomeres lacking TRF2, and the repair of DSBs in BRCA1-deficient cells treated with PARP inhibitors [7, 8]. In mice, loss of REV7, SHLD2, or SHLD1 does not impact lymphocyte development nor V(D)J recombination [12–14]. By contrast, SHLD-deficient B cells exhibit severe CSR defects, due to uncontrolled resection of AID-induced DSB ends that results in the accumulation of aberrant nonproductive switched products and unrepaired chromosomal breaks at *Ig* switching sites [12–14].

The link between SHLD and CST and its precise role in CSR remains unclear. In CH12F3 B cells, a lymphoma B cell line inducible for IgM-to-IgA class switching [15], CTC1 heterozygosity leads to decreased CSR [16] and CTC1-deficient murine splenic B cells show reduced class switching [17], indicating that CST contributes to CSR. Recent work identified 4 amino acids (LDLP at position 18–21) in the N-terminal region of SHLD1 that mediates SHLD1-CTC1 interaction. SHLD1$^{\Delta LDLP}$ mutant, possessing the deletion of these 4 amino residues, phenocopies SHLD1-null cells in the context of BRCA1 deficiency and fails to recruit CST to irradiation-induced DNA damage foci [10]. In contrast, SHLD1$^{\Delta LDLP}$ represses the formation of excessive single-stranded 3′ DNA at telomeres similar to wild-type SHLD1 [10]. SHLD1$^{\Delta LDLP}$ also sustains normal IgM-to-IgA CSR in stimulated CH12F3 B cells [10] and IgM-to-IgG1 CSR in stimulated primary B cells [12], indicating that SHLD1-CTC1 interaction through this motif is dispensable for CSR. In this study, we aim to clarify the role of CST and its interplay with SHLD during CSR. In

particular, we tested the capacity of SHLD1$^{\Delta LDLP}$ to perform class switching at multiple isotypes and investigated the role of CST in genome stability, DSB end resection, and DSB repair pathway choice. We find that SHLD1$^{\Delta LDLP}$ promotes productive Ig class switching to multiple isotypes in primary B cells, firmly demonstrating that the LDLP motif of SHLD1 is dispensable for CSR. Using *Ctc1, Stn1, Shld1,* and *Shld2* knockout CH12F3 B cells, we show that CST and SHLD are both required for CSR. Finally, we show that CTC1 and SHLD1 act epistatically during CSR by limiting genetic instability, DSB end-resection, and alternative microhomology-mediated end-joining at Ig switching sites.

2 | Results and Discussion

2.1 | SHLD1$^{\Delta LDLP}$ and SHLD1^{L20A} Undergo Efficient IgM to IgA, IgG1, IgG2b and IgG3 Class Switching

The IgA switch region contains over 60 copies of tandem pentamers ATGGG and GAGGA (Figure S1A,B). CST is known to bind canonical G-rich repetitive sequences present at telomeres [TTAGGG] and G-rich sequences that deviate from these telomere repeats [18]. Thus, the IgA locus might represent a good substrate for CST, as in the case of telomeres. Consistent with this, it was shown by EMSA assay that CST can specifically bind both G-rich sequences of the core IgA switch region and G-rich sequences mimicking telomere repeats [9]. It is however unclear whether SHLD1$^{\Delta LDLP}$ retains its ability to promote CSR at other isotypes for which switch regions are different in terms of repeat length and content [3] (Figure S1). Therefore, we tested SHLD1$^{\Delta LDLP}$ and SHLD1^{L20A}, a second SHLD1 mutant protein predicted to alter SHLD1-CTC1 interaction [10], for their ability to rescue CSR in *Shld1$^{-/-}$* primary B cells stimulated with isotype-specific cytokines to induce CSR to multiple isotypes in parallel (Figure 1A). SHLD1$^{\Delta LDLP}$ and SHLD1^{L20A} (Figure S2A) were expressed at similar levels as wild-type SHLD1 (SHLD1) (Figure S2B,C). Consistent with previous findings [12], expression of SHLD1$^{\Delta LDLP}$ or SHLD1^{L20A} restored IgM-to-IgG1 to the same extent as SHLD1 (Figure 1B,C). Similarly, we find that SHLD1$^{\Delta LDLP}$ and SHLD1^{L20A} fully restore CSR to IgG2b (Figure 1D), IgG3 (Figure 1E), and IgA (Figure 1F). As expected [10], SHLD1$^{\Delta LDLP}$ and SHLD1^{L20A} also behave like SHLD1 when tested for IgM-to-IgA CSR in CH12F3 B cells (Figure S2D–H). A significant fraction of SHLD-deficient B cells lose expression of Ig upon induction of CSR (Ig-negative B cells, Ig^{neg}) [12, 13]. This loss of Ig is due to CSR coupled with overactive resection, inversion, or lack of repair [12, 13]. Next, we quantified the proportion of Ig^{neg} cells in *Shld1$^{-/-}$* B cells complemented with SHLD1, SHLD1$^{\Delta LDLP}$, or SHLD1^{L20A} after induction of CSR for 5 days. In stimulated wild-type (WT) B cells and *Shld1$^{-/-}$* B cells complemented with full-length SHLD1, Ig^{neg} B cells represented 5 to 10% of total B cells, depending on the Ig switching conditions (Figure 1B,G–J). By contrast, the fraction of Ig^{neg} B cells augmented to 20 to 30% in *Shld1$^{-/-}$* B cells or *Shld1$^{-/-}$* B cells complemented with an empty expression vector (Figure 1B,G–J). Expression of SHLD1$^{\Delta LDLP}$ or SHLD1^{L20A} in *Shld1$^{-/-}$* B cells restored the percentage of Ig^{neg} B cells to 5 to 10% of total B cells (Figure 1B,G–J), confirming that these mutant proteins act as wild-type SHLD1 during CSR. Together these results demonstrate that SHLD1$^{\Delta LDLP}$ is fully
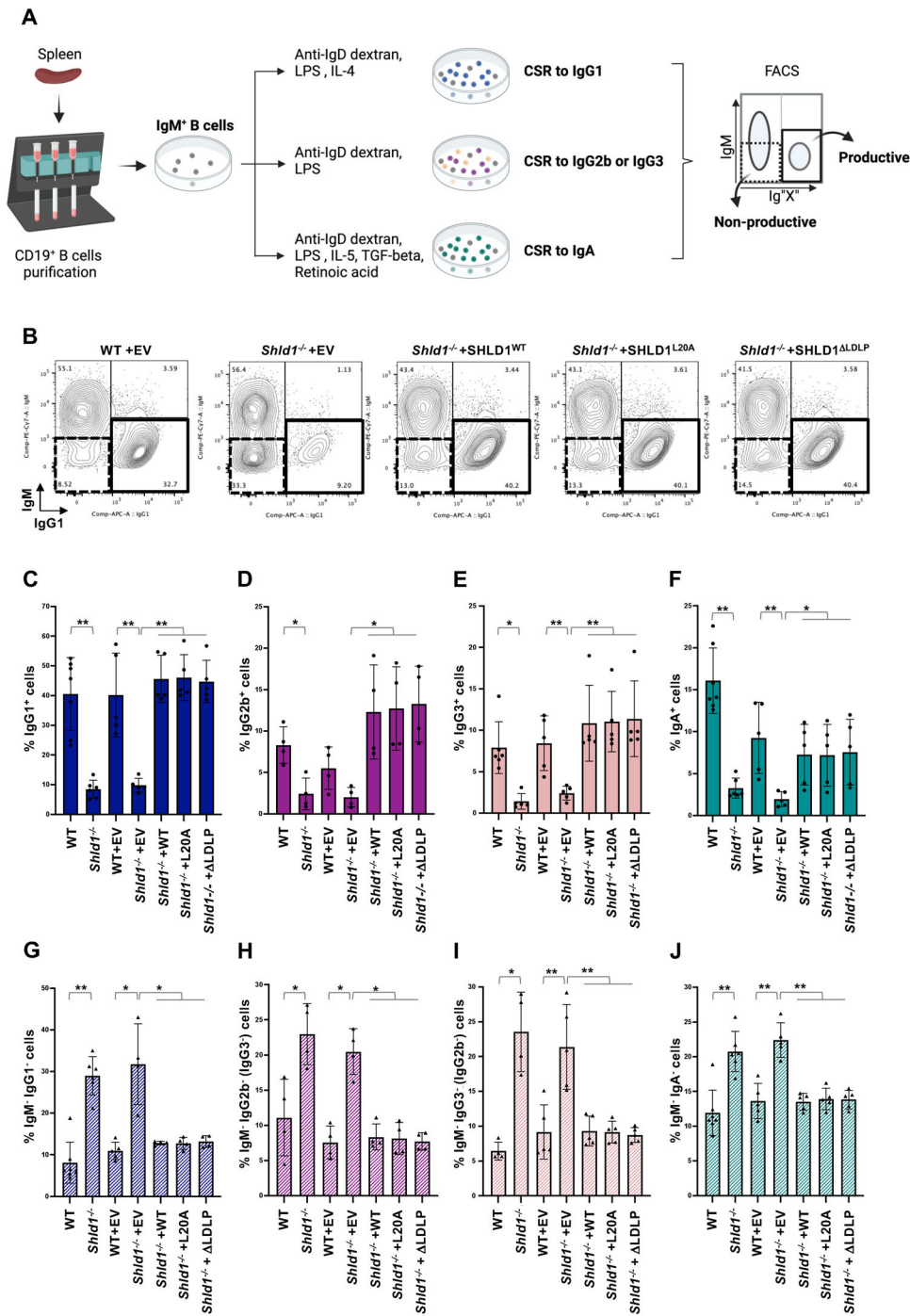
FIGURE 1 | SHLD1-CTC1 interaction via the SHLD1 LDLP motif is dispensable for CSR. (A) Schematic of the experimental workflow was done using Biorender. (B) Representative FACS plots of IgG1 CSR assay in primary B cells of the indicated genotype. IgG1^{+} and Ig^{neg} cells are highlighted with black lines and dashed black lines respectively. (C–F) Percentages of IgG1^{+} (C), IgG2b^{+} (D), IgG3^{+} (E), and IgA[+] (F) cells in controls and $Shld1^{-/-}$ primary B cells complemented with empty vector (EV) or SHLD1 variants. (G–J) Percentages of nonproductive IgM[low] IgG1^{−} (G), IgM[low] IgG2b^{−} (IgG3^{−}) (H), IgM[low] IgG3^{−} (IgG2b^{−}) (I) and IgM[low] IgA[−] (J) fractions in controls and $Shld1^{-/-}$ primary B cells complemented with SHLD1 variants. Bars represent the mean ± SD. $n = 4$–7 for WT; $n = 4$–6 for $Shld1^{-/-}$; $n = 4$–5 for WT+EV, $Shld1^{-/-}$ +EV, $Shld1^{-/-}$ + SHLD1[WT], $Shld1^{-/-}$ + SHLD1[L20A], and $Shld1^{-/-}$ + SHLD1[ΔLDLP]. ***$p < 0.001$; **$p < 0.01$; *$p < 0.05$. Mann–Whitney test.

competent for CSR, regardless of the class switch isotype tested. This led us to propose two models: 1) CST is dispensable for CSR with 53BP1-RIF1-SHLD being self-sufficient to limit resection of AID-DSB ends and promote productive CSR, and 2) CST acts during CSR through a mechanism that is independent of its interaction with SHLD1 through the LDLP motif.

2.2 | CST Is Required for *Igh* CSR and Is Epistatic With SHLD

To test these two models, we generated knockout CH12F3 B cell clones for the *Ctc1*, *Stn1*, and *Shld1* genes, along with $Shld1^{-/-}$ $Ctc1^{-/-}$ double knockout B cell clones (Figure S3). Notably, we

were able to efficiently generate multiple *Ctc1* and *Stn1* knockout B cell clones (Figure S3, Table S1). While these results contrast with previous attempts to generate *Ctc1* null CH12F3 B cell clones [16], they are consistent with a recent study reporting that CTC1 is dispensable for B cell development [17]. To avoid any potential long-term proliferation defect due to the absence of telomeric CST [19], we performed our experiments within a month after generating knockout B cell clones. Within this timeframe, *Stn1* and *Ctc1* knockout B cell clones grew similarly to wild-type CH12F3 B cell clones, with no difference in doubling time or cell cycle profile (Figure 2A,B; Figure S4A–D). To assess CSR levels in the absence of STN1 or CTC1, we stimulated WT, *Stn1*−/−, *Ctc1*−/−, *Shld1*−/−, and *Shld1*−/− *Ctc1*−/− CH12F3 B cells, together with previously generated *Shld2*−/− CH12F3 B cells [20], for IgM-to-IgA class switching with α-CD40, IL-4 and TGF-β cytokines (CIT) (Figure 2A). Flow cytometry assays for surface IgA revealed strong and similar defects in CSR in *Stn1*−/−, *Ctc1*−/−, *Shld2*−/− and *Shld1*−/− B cells compared with WT cells, with *Shld1*−/− cells having the most severe phenotype among all genotype tested (Figure 2C,D). Average levels of IgA in STN1- and CTC1-deficient B cell clones were at roughly 43% of those of WT controls while IgA levels in *Shld2*−/− and *Shld1*−/− B cells were at about 37% and 25% of those of WT, respectively (Figure 2D). A large fraction of stimulated *Stn1*−/− and *Ctc1*−/− B cells also lost Ig expression at the cell surface, similar to *Shld2*−/− and *Shld1*−/− B cells (fraction of Ig^{neg} cells: WT, 5.3%; *Stn1*−/−, 28.7 %; *Ctc1*−/−, 30.1%; *Shld2*−/−, 28.6%; *Shld1*−/−, 28.5%) (Figure 2E). To determine whether CST and SHLD have distinct synergistic functions or are epistatic during CSR, we measured CSR levels in SHLD1/CTC1 double-deficient B cells. CTC1/SHLD1-deficient cells switched to IgA and accumulated Ig^{neg} cells to the same extent as *Shld1*−/− cells, demonstrating that SHLD and CST are epistatic during CSR (Figure 2C–E). Importantly, CSR defects observed in STN1-, CTC1-, SHLD2-, SHLD1-, and double SHLD1/CTC1-deficient B cells were not due to defects in cell proliferation, cell cycle distribution, or germline transcripts expression (Figure 2B; Figure S4A–F) [20]. Moreover, complementation of *Ctc1*−/− cells with wild-type CTC1 fully restored CSR and Ig^{neg} percentage to WT levels in these cells (Figure S4G–J). From these results, we conclude that CST is essential for CSR and is epistatic to SHLD1.

As SHLD1$^{\Delta LDLP}$ supports CSR, these results suggest that CST may act at DSB ends without being directly recruited by SHLD1. Consistent with this, a recent AlphaFold2 analysis of human SHLD and CST complexes predicted an interaction between CTC1 and the third OB fold of SHLD2 that is compatible with SHLD1-SHLD2 binding [21]. SHLD2 might thus serve as an interface for CST recruitment during CSR, in a similar way to the Shelterin protein POT1 which recruits CST-Polα-primase to telomeres [22]. If SHLD2 is sufficient for CST-Polα-primase recruitment, then why do SHLD1-deficient cells have such a defect in CSR? It was reported that SHLD1 promotes the formation of SHLD2 irradiation-induced foci [20]. Thus, it is possible that SHLD1-deficient B cells also suffer abnormal SHLD complex assembly at AID-DSBs, which might compromise CST-Polα-primase recruitment and CSR.

2.3 | CTC1 and SHLD1 Are Epistatic in Promoting Repair and Limiting Resection of AID-Induced DSB Ends

Next, we investigated the mechanisms underlying the CSR defects observed in CST-deficient cells using knockout B cell clones for *Ctc1*, *Shld1*, or both genes. Diminished CSR in SHLD1-deficient B cells is associated with an accumulation of unrepaired AID-induced DNA breaks and overactive DNA end resection [12]. To test whether similar defects account for the observed decrease in CSR levels in *Ctc1*−/− B cells, we first measured the percentage of *Igh* chromosome breaks and translocations by performing *Igh* locus-specific DNA–FISH on chromosome spreads prepared from WT, *Ctc1*−/−, *Shld1*−/−, and *Shld1*−/− *Ctc1*−/− CH12F3 B cells in both control and stimulating IgM-to-IgA class switching conditions (Figure 3A,B). Analysis of hundreds of metaphase spreads from independent B cell clones revealed low levels of spontaneous *Igh* locus-associated chromosome instability across all genotypes (WT, 1%; *Ctc1*−/−, 2.5%; *Shld1*−/−, 4.2%; *Shld1*−/− *Ctc1*−/−, 3.3%). WT cells stimulated for CSR also harbored low levels of *Igh* locus instability (3.3%). However, stimulated *Ctc1*−/− B cells showed a significant 10-fold increase in aberrant metaphases (27%), consisting of chromosome breaks (21.7%) and translocations (5.4%) (Figure 3B; Table S2). In addition, stimulated *Shld1*−/− *Ctc1*−/− and *Shld1*−/− B cells harbored similar levels of aberrant metaphases (35.1% and 30.9% respectively, Figure 3B), which is in line with the CSR defects observed above in these cell clones (Figure 2F,G). Next, we applied a long-range PCR (LR-PCR) approach to detect resection at AID-targeted switch sites [12, 13]. This LR-PCR amplifies a region between the *Igh* intronic enhancer iEμ and the *Ighα* constant exon 4 (Figure 3C). CH12F3 B cells harbor an already rearranged nonproductive allele that is readily amplified with this assay (8.1 kb amplicon detected in *Aid*−/− B cells; Figure 3C,D; Figure S5A) [15, 23]. Amplification of genomic DNA from stimulated WT cells generated a thicker band whose size corresponds to the unproductive rearranged allele as well as to the expected deletional recombination products between the Sμ region and the Sα region on the productive allele, ranging from 5.1–13.5 kb. Strikingly, compared with WT cells, *Ctc1*−/− cells harbored recombination products of various smaller sizes as visualized by a smear on the agarose gel (Figure 3D; Figure S5A). A similar smear was also observed in *Shld1*−/− cells, reflecting long-range resection of AID-induced DSB ends prior to joining (Figure 3D; Figure S5A) [12]. In addition, we obtained similar profiles in *Shld1*−/− *Ctc1*−/− cells, suggesting that CTC1 and SHLD1 both protect against DSB end resection at *Ig* switching sites in an epistatic manner. To analyze resection and breakpoint junction features more precisely, we sequenced PCR products using long-read high-throughput PacBio sequencing. In WT B cells, most of the sequences corresponded to recombination products with breakpoint sites mapping within Sμ and Sα regions (median read length: 7.379 kb) (Figure 3E; Figure S5B,C). Consistent with the gel profiles, the mapped recombination products were smaller for CTC1-deficient cells (median read length: 5.696 kb). In SHLD1/CTC1-deficient cells, recombination products were similar in size to those in SHLD1-deficient cells (median read length: 5.317 and 5.080 kb, respectively) (Figure 3E;
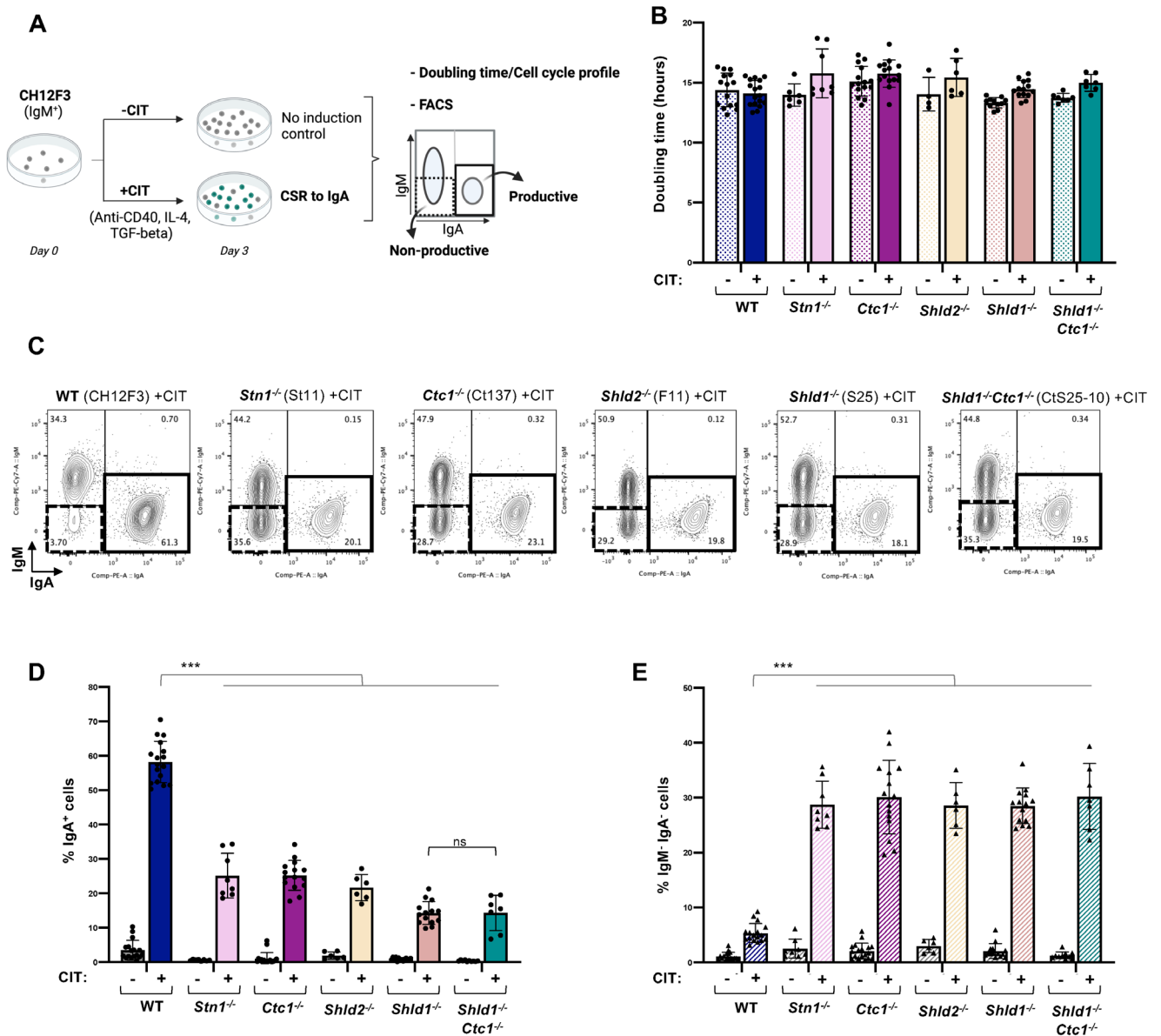
FIGURE 2 | CST is required for CSR and is epistatic with SHLD. (A) Schematic of the experimental workflow was done using Biorender. (B) Doubling time for untreated cells (-CIT) and stimulated cells (+CIT) of the indicated genotype. Bars represent the mean ± SD. (C) Representative FACS plots of IgA CSR assay in the indicated CH12F3 clones. IgA$^+$ and Ig^{neg} cells are highlighted with black lines and dashed black lines respectively. (D) Percentages of IgA$^+$ CH12F3 cells with and without in vitro stimulation for 3 days for the indicated genotypes. (E) Percentages of IgM$^-$ IgA$^-$ CH12F3 cells with and without stimulation for 3 days for the indicated genotypes. Bars represent the mean ± SD of at least three independent experiments. Two clones for WT (CH12F3 and Ct34), 3 clones for $Stn1^{-/-}$ (St11, St17, St20), 8 clones for $Ctc1^{-/-}$ (Ct10, Ct11, Ct21, Ct105, Ct131, Ct137, Ct160, Ct168), 2 clones for $Shld2^{-/-}$ (F11, F12), 3 clones for $Shld1^{-/-}$ (O6, S8, S25), and 4 clones for $Shld1^{-/-}$ $Ctc1^{-/-}$ (CtS25-4, CtS25-6, CtS25-10, CtS8-4) were used. ***$p < 0.001$, Mann–Whitney test. CIT: anti-CD40, IL-4, TGF-β.

Figure S5B,C). To avoid potential bias introduced during the LR-PCR and sequencing procedures and, by the presence of the already rearranged nonproductive allele, only unique breakpoints with a ≥10× sequencing depth were used for downstream analysis of DSB breakpoint junction location and signature. The PCR product from the nonproductive rearranged allele was therefore counted as a single rearrangement event among thousands of unique reads: 6149, 8645, 4976, and 4769 junctions analyzed in WT, $Ctc1^{-/-}$, $Shld1^{-/-}$, and $Shld1^{-/-}$ $Ctc1^{-/-}$ cells, respectively (Table S3). Sμ and Sα regions were defined as regions located between the I promoter and the corresponding constant exons

(Figure 3C) [24]. In WT cells, resected products with breakpoint junctions mapping outside the switch regions represented only 19.4 % of the junctions (Figure 3F,G; Table S3). By contrast, the percentage of resected joints increased to 47.7% in $Ctc1^{-/-}$ cells and 54.9% in $Shld1^{-/-}$ cells (Figure 3G). Resection tracks extended up to the EμF and CαR primers in both $Ctc1^{-/-}$ cells and $Shld1^{-/-}$ cells (Figure 3F), indicating similar long-range resection activity in the absence of CTC1 or SHLD1. In agreement with previous studies [12], junctions were approximately 30% direct (i.e., junctions that do not contain MH) in WT cells (Figure 3H,J; Table S3). Direct junctions decreased to 24.8% and
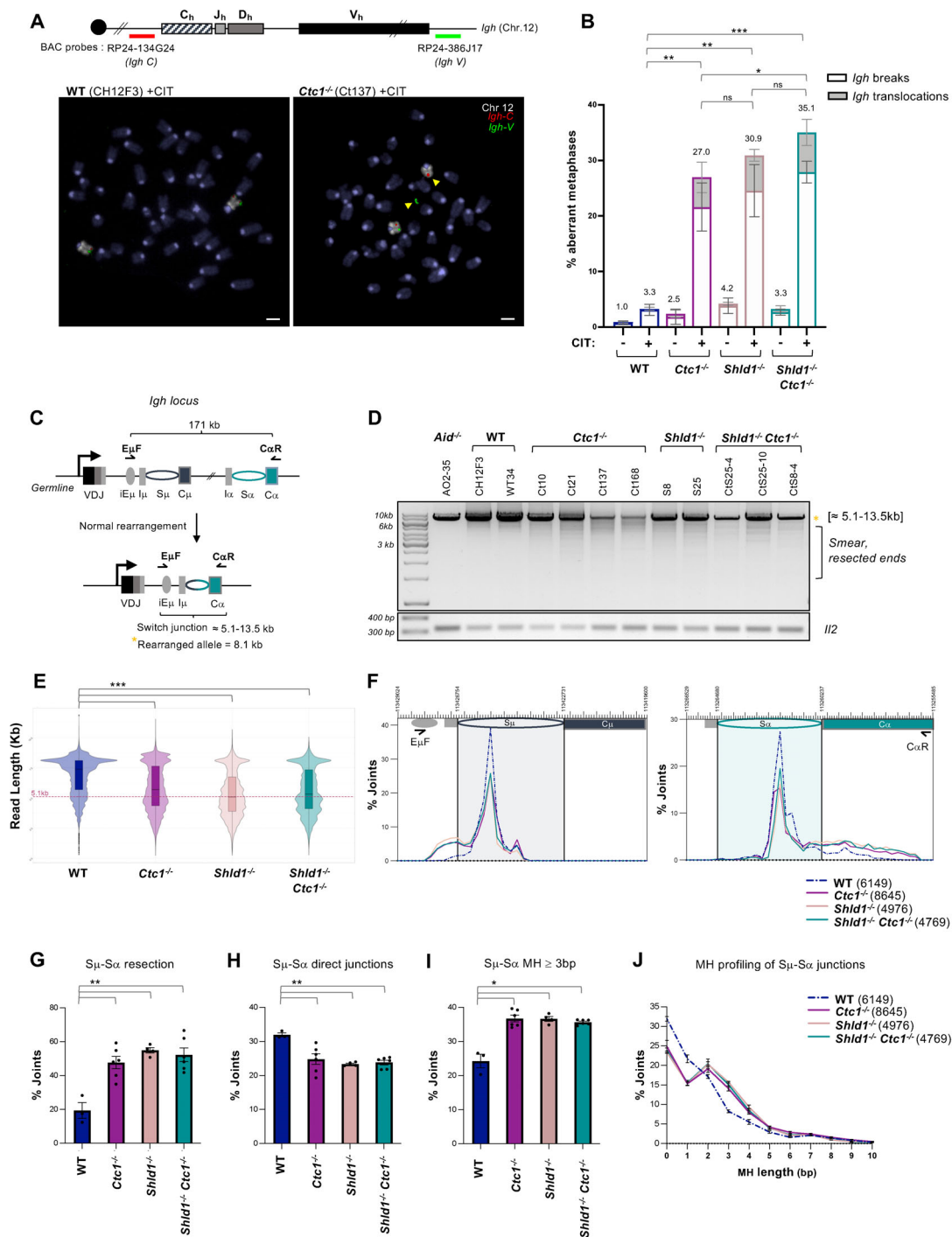
FIGURE 3 | CTC1 and SHLD1 are epistatic in promoting DSB repair and limiting DSB end resection during CSR. (A) Representative images of metaphase spread from WT cells (left panel) and $Ctc1^{-/-}$ cells (right panel, yellow triangles point to a broken chromosome at the Igh locus), as quantified in (B), scale bars, 3 μm. (B) Quantification of Igh breaks (white bar) and translocations (grey bar) in metaphases of WT, $Ctc1^{-/-}$, $Shld1^{-/-}$ and $Shld1^{-/-}$ $Ctc1^{-/-}$ cells with or without stimulation for 3 days. Bars represent means $\pm$ SD. See also Table S2. ***$p < 0.001$; **$p < 0.01$; *$p < 0.05$, Student t-test. (C) Schematic representation of the murine Igh locus. Arrows indicate primers used for the long-range PCR. (D) Long-range PCR analysis of Sμ to Sα rearrangements in WT, $Ctc1^{-/-}$, $Shld1^{-/-}$, and $Shld1^{-/-}$ $Ctc1^{-/-}$ stimulated CH12F3 cells (Replicate 1). $Il2$ gene PCR was used as a loading control. See also Figure S5. (E) Length distribution of mapped PacBio reads from long-range PCR. Samples from replicates 1 and 2 were pooled per genotype. See also Figure S5. ***$p < 0.001$; mixed-model regression test. (F) Analysis of breakpoints localization. Graphs represent the percentage of junctions. Sμ and Sα switch regions are colored light grey and light green respectively. Coordinates on mm10 are indicated. The total number of unique junctions analyzed for each genotype is indicated in brackets. (G) Percentage of resected Sμ–Sα junctions. A junction was categorized as resected when the breakpoint was mapped outside of either Sμ or Sα as defined in (F). Bars represent mean $\pm$ SEM. **$p < 0.01$, Student t-test. (H) Percentage of Sμ–Sα direct junctions. Bars represent mean $\pm$ SEM. **$p < 0.01$, Student t-test. (I) Percentage of Sμ–Sα junctions with ≥ 3 bp microhomologies (MH). Bars represent mean $\pm$ SEM. *$p < 0.05$, Student t-test. (J) MH usage distribution of Sμ–Sα junctions. Graphs represent mean $\pm$ SEM. WT, $n = 3$; $Ctc1^{-/-}$, $n = 6$; $Shld1^{-/-}$, $n = 5$; $Shld1^{-/-}$ $Ctc1^{-/-}$, $n = 6$. The total number of unique junctions analyzed for each genotype is indicated in brackets.

23.4% in *Ctc1*$^{-/-}$ cells and *Shld1*$^{-/-}$ cells, respectively (Figure 3H,J; Table S3). Both *Ctc1*$^{-/-}$ cells and *Shld1*$^{-/-}$ cells displayed an increase in MH-mediated junctions with respectively 36.8% and 36.7% of the joints harboring ≥3 bp MH compared with 24.3% in WT cells (Figure 3I,J; Table S3). These results are consistent with previous findings showing increased MH-mediated end-joining in SHLD-deficient B cells [12, 13, 25] and indicate that both CTC1 and SHLD1 limit MH-mediated alternative end-joining during CSR. In agreement with this, both *Ctc1*$^{-/-}$ and *Shld1*$^{-/-}$ stimulated B cells displayed increased chromosomal translocations (Figure 3B), another hallmark of alternative end-joining that is observed in the absence of NHEJ [26, 27]. These observations suggest that SHLD and CST impact—directly or indirectly—on the recruitment of NHEJ factors at AID DSBs sites. Breakpoint joints recovered from double SHLD1/CTC1-deficient cells were indistinguishable from those recovered from SHLD1-deficient cells in their localization, resection length, and MH usage (Figure 3F–J). Thus, we conclude that CTC1 is required for CSR by antagonizing DNA end resection and promoting NHEJ DNA repair in a manner that is epistatic to SHLD1.

The epistatic actions of SHLD and CST during CSR support a model in which SHLD recruits CST-DNA polymerase α (Polα)-primase to promote fill-in DNA synthesis at DSB ends [9]. However, the participation of Polα-primase-mediated fill-in synthesis in *Ig* class switching remains to be determined, which is challenging due to the requirement of these factors for cell division, a prerequisite for CSR. CST evolved from an archaeal replication protein A (RPA, composed of the Rpa1, Rpa2, and Rpa3 subunits in archaea; RPA70, RPA32, and RPA14 in humans), with the CTC1 subunit containing seven tandem OB folds with structural homologies with the four OB folds of RPA70 [28, 29]. CTC1 binding to ssDNA through its OB-folds might thus directly protect AID-DSB ends against the action of nucleases, limiting exacerbated resection independently of Polα. RPA is also known to interact with AID and UNG and regulates DNA deamination and mutagenic uracil processing at *Ig* loci [30, 31]. One can speculate that CST replaces RPA in the transition from the deamination phase to the repair phase during CSR. In addition, CST is known to limit G-quadruplex (G4) accumulation at telomeres and other genome sites [9, 32] possibly by assembling as a decamer structure that could act as a nucleosome equivalent for G-rich ssDNA [29]. As G4 structures are present within switch regions and are implicated in AID targeting and class switching [33], the regulation/disassembly of G4 by CST might also be required for the proper repair of AID-induced DSB ends.

3 | Conclusion

In summary, our findings demonstrate the importance and interdependence of the SHLD and CST complexes in promoting productive DSB end-joining and maintaining genome stability during CSR. They also raise questions as to the specific modes of action of these complexes and their dynamics during Ig class switching, paving the way for future investigations.

4 | Data Limitations and Perspectives

Long-range resection measurements are based on the analysis of junctions, i.e. post-recombination events. A more direct measurement of resection by DSB/ssDNA end-sequencing or RPA ChIP-sequencing techniques has not been performed in this study and might provide complementary information. In addition, although the SHLD1$^{\Delta LDLP}$ protein fully rescues CSR levels in SHLD1-deficient B cells, we did not analyze switched recombination products in SHLD1$^{\Delta LDLP}$ cells and thus cannot rule out that it partially affects DSB pathway choice during CSR.

5 | Experimental Procedures

5.1 | Mice

Shld1$^{-/-}$ mice were described previously [12]. Mice were bred under specific-pathogen-free conditions and housed at ambient temperature and humidity with 12 h light/12 h dark cycles. In all experiments, 8–12-week-old mice were used. All experiments were performed in accordance with the guidelines of the institutional animal care and ethical committee of Institut Pasteur/CETEA n°89 under protocol numbers 220060/39309.

5.2 | Ex Vivo CSR Assay

Splenic B-cells were purified from 8–12-week-old mice using magnetic CD19 beads according to the manufacturer's instructions (Miltenyi Biotec). 1.2×10^6 cells were cultured in 2 mL of complete medium consisting of RPMI 1640 supplemented with 12% FBS, penicillin (100 U/mL)/streptomycin (100 μg/mL), 50 μM 2-mercaptoethanol and incubated at 37°C in a humidified atmosphere containing 5% CO_2. To induce specific isotype switching, B cells were stimulated with either LPS (25 μg/mL, Sigma Aldrich), IL-4 (10 ng/mL, Miltenyi) and anti-IgD dextran (6 ng/mL, Fina Biosolutions) for IgG1, LPS and anti-IgD dextran for IgG2b and IgG3, or LPS, anti-IgD dextran, IL-5 (5 ng/mL, Biotechne), TGFβ (3 ng/mL, R&D Systems), and retinoic acid (0.3 ng/mL, Sigma Aldrich) for IgA. After 36 h, cells were infected with retroviral-based vectors expressing wild-type and mutant forms of SHLD1 or the empty vector. At day 5, cells were assayed for class-switching by flow cytometry using B220-A488 (RA3-6B2, 1:200 dilution), B220-APC (RA3-6B2, 1:200 dilution), IgG1-APC (X56, 1:500 dilution), IgG2b-PE (RMG2b-1, 1:500 dilution), IgG3-FITC (R40-82, 1:500 dilution), IgA-PE (mA-6E1, 1:200 dilution), IgM-PE-Cy7 (R6-60.2, 1:200 dilution), Thy1.1-BV421 (HIS51, 1:300 dilution) antibodies, and a Fortessa analyzer (BD Biosciences). For FACS analysis of Ig-positive and Ig-negative populations in complemented cells, cells were first gated on THY1.1 expression using Thy1.1-BV421 antibody (HIS51). Data were analyzed by FlowJo software v10.4.2 (TreeStar). Viable cells were counted using a Casy cell counter (Roche).

5.3 | Culture and CRISPR/Cas9 Editing of CH12F3 Cell Lines

CH12F3 cells were cultured in RPMI 1640 supplemented with 12% FBS (Sigma F7524), penicillin (100 U/ml)/streptomycin (100 μg/mL), 50 μM 2-mercaptoethanol, 1× MEM nonessential amino acids, 1 mM sodium pyruvate, and 10 mM Hepes. CH12F3 knockout cell clones were generated as previously described [12]. Briefly, cells were nucleofected with a double sgRNAs-encoding

plasmid containing SpCas9 and GFP (see Table S4 for sgRNAs sequences) using an Amaxa Nucleofector and Nucleofector Kit SF solution (Lonza). Electroporated cells were left to recover for 36–48 h and single cells expressing GFP were sorted in 96-well plates. Clones were then screened by PCR (see Table S4 for primers sequences), and purified PCR products were Sanger sequenced to identify CRISPR/Cas9-induced deletions and insertions at the cleavage site (see Table S1).

5.4 | CSR Assay in CH12F3 Cell Lines

CH12F3 cells were plated at 50,000 cells per ml in complete RPMI supplemented with anti-CD40 antibody (1 µg/mL, Miltenyi), IL-4 (20 ng/mL, Miltenyi), and TGF-β (1 ng/mL, R&D Biotech) to induce IgM to IgA switching. After 3 days, viable cells were counted using a Casy cell counter (Roche) and assayed for class-switching by flow cytometry using IgA-PE (mA-6E1, 1:200) and IgM-PE-Cy7 (R6-60.2, 1:200 dilution) antibodies, and a Fortessa analyzer (BD Biosciences). Data were analyzed by FlowJo software v10.4.2 (TreeStar). For SHLD1 and CTC1 complementation, $Shld1^{-/-}$ or $Ctc1^{-/-}$ cells were infected with a retroviral-based vector expressing SHLD1 (WT or mutant) and THY1.1 or CTC1 and THY1.2 before stimulation. For FACS analysis of IgA$^+$ and IgM$^-$IgA$^-$ populations in complemented cells, cells were first gated on THY1.1 or THY1.2 expression using Thy1.1-BV421 (OX-7, 1:200) or Thy1.2-APC (53-2.1, 1:200) antibody.

5.5 | Retroviral Vector Production and Complementation of CH12F3 Clones

Human *Shld1* cDNA was cloned into MSCV-IRES-Thy1.1 plasmid from Addgene (17442) to produce MSCV-Shld1-IRES-Thy1.1 plasmid encoding for SHLD1 and the cell surface marker THY1.1. This plasmid was then modified by site-directed mutagenesis to generate SHLD1$^{\Delta LDLP}$ and SHLD1^{L20A} expressing plasmids (Genewiz). Mouse *Ctc1* cDNA was obtained from Origene Technologies (MR220024) and cloned into MSCV-IRES-Thy1.2 retroviral vector, previously generated from MSCV-IRES-Thy1.1 plasmid from Addgene (plasmid #17442), to produce MSCV-Ctc1-IRES-Thy1.2 plasmid encoding for CTC1 and the cell surface marker THY1.2. Amphotropic retroviral supernatants were prepared by transfection of Platinum-A cells (RV-102) with 20 µg of plasmid using Lipofectamine LTX (Invitrogen). Retroviral supernatants were harvested 48 h after Plat-A transfection, snap-frozen, and conserved at −80°C. SHLD1-deficient cells were infected with either empty MSCV-IRES-Thy1.1 or MSCV-Shld1-IRES-Thy1.1 retroviral supernatant and CTC1-deficient cells were infected with either empty MSCV-IRES-Thy1.2 or MSCV-Ctc1-IRES-Thy1.2 retroviral supernatant using spin-infection and subsequently assayed for CSR. THY1.1 or THY1.2 positive cells were identified using Thy1.1-BV421 (OX-7, 1:200) or Thy1.2-APC (53-2.1, 1:200) antibody and eventually purified using magnetic Thy1.1 or Thy1.2 beads according to the manufacturer's instructions (Miltenyi Biotec).

5.6 | Western Blotting

Cells were lysed using RIPA cell lysis reagent (Thermo Fisher Scientific 89900) and protease inhibitors cocktail (Roche

11873580001). Equal amounts of proteins were subjected to SDS-PAGE on 10% Bis-Tris gel. Proteins were transferred onto a nitrocellulose membrane (Life Technologies) using the iBlot apparatus (P3 program, 7 min transfer, Invitrogen). Membranes were incubated in 5% nonfat dried milk in TBS containing 0.1% Tween-20 buffer for at least 1 h at room temperature, and subsequently incubated overnight at 4°C with SHLD1 primary antibody (Thermo Fisher Scientific PA5-59280, 1:200) or STN1 antibody (Santa Cruz sc-376450 HRP, 1:250). γ-Tubulin (Sigma Aldrich T6557, clone GTU-88, 1:10000) was used as a loading control. HRP-conjugated anti-rabbit secondary antibody (Cell Signaling Technology 7074, 1:2500) or HRP-conjugated anti-mouse secondary antibody (Cell Signaling Technology 7076, 1:20000) were used. Immune complexes were detected with Clarity Western ECL Substrate (Biorad) or WesternBright Sirius substrate (Advansta). Blots were developed and analyzed using Image Lab v6.0 (Biorad).

5.7 | Cell Cycle Assay

CH12F3 cells were incubated with 100 µM Edu (Jena Bioscience CLK-N001-25) for 1 h at 37°C and washed once with PBS. Cells were then fixed with 2% paraformaldehyde at 4°C for at least 24 h and washed once with PBS. Cells were stained with 1 mM CuSO4 (Sigma C1297-100G), 2 µM iFluor 647 azide (AAT Bioquest 1091), and 100 mM l-Ascorbic acid (Sigma A5960-25G) for 1 h at room temperature. After one wash with PBS, cells were incubated with PI staining cocktail (1.9 mM sodium citrate tribasic dehydrate (Sigma S4641-500G), 25 µg/mL propidium iodide (ThermoFisher Scientific 440300250), 250 µg/mL RNAse A (Invitrogen 8003089), 0.5 mM Tris-Hcl, 0.75 mM NaCl) O/N at 37°C. Finally, cells were centrifuged and resuspended in PBS for FACS analysis. FACS data were acquired on a Fortessa analyzer (BD Biosciences) and analyzed and visualized by Flowjo software v10.4.2 (TreeStar).

5.8 | RT-qPCR

RNA was extracted from CH12F3 cells after 2 days of stimulation using the RNeasy kit and on-column DNase digestion (Qiagen 74104 and 79254). cDNA was obtained from 2 µg total RNA using the High-Capacity cDNA Reverse Transcription kit (Applied Biosystems 4368814). *Igh* μ germ-line transcripts (GLTμ) and *Igh* α germ-line transcripts (GLTα) quantitative PCR (qPCR) were performed in duplicates using SYBR Green PCR Master mix (Applied Biosystems 4309155) and primers listed in Table S4 as previously described [34]. Transcript quantities were normalized to *Actin* mRNA.

5.9 | DNA FISH on Metaphase Spreads

DNA FISH was performed as previously described [35]. Slides were treated with RNase A for 40 min, dehydrated in 70, 90, and 100% ethanol for 3 min each, denatured in 70% formamide/2× SSC for 3 min at 77°C, dehydrated again in cold ethanol series, and hybridized with probes overnight at 37°C in a humid chamber. The next day, slides were washed three times in 50% formamide/0.5× SSC for 5 min each at 37°C and twice in 0.5× SSC for 10 min and 20 min at 37°C. Finally, slides were mounted

in ProLong Gold antifade reagent with DAPI (Invitrogen P36931) to counterstain total DNA. Metaphases were imaged using a ZEISS AxioImager.Z2 microscope and the Metafer automated capture system (MetaSystems) and counted manually. Probes used in this study: *Igh C* BAC probes (RP24–134G24), *Igh V* BAC probe (RP24–386J17), and XCyting Mouse Chromosome 12 paint (MetaSystems).

5.10 | LR-PCR and Pacbio Sequencing

Long-range PCR of the *Ighµ-Ighα* amplicon was accomplished using Platinum SuperFi II polymerase Master Mix (Invitrogen 16445389). A total of 300 ng of gDNA was amplified in 150 µL using EµF and CαR primers and the following cycles: 1× (98 °C 30 s); 30× (98°C 10 s, 57°C 10 s, 72°C 8 min); 1× (72°C 5 min). See Table S4 for primer sequences. For each sample, bulk PCR amplicons were purified, and sequencing libraries were prepared, prior to sequencing using the long-read PacBio Revio technology by Novogene. Sequences were demultiplexed and HiFi reads were constructed using the consensus circular reads workflow implemented in SMRTLINK software from PacBio (v9) (smrtlink: https://www.pacb.com/support/software-downloads/). After the conversion of HiFi reads into FastQ files, they were mapped onto the Mus musculus genome (reference GRCm38) using minimap2 v2.26-r1175 including PacBio and splicing options. Reads that did not align to both 5′ and 3′ sections of the region of interest (chromosome 12, 113255485 - 113431785) were filtered out. Subsequent bioinformatics analysis of the aligned reads was performed with SAMtools and R for coverages and read lengths, while junction analyses were conducted using in-house bash/awk and R scripting. Briefly, for each read, the breakpoint spanning from 5′ (Sα regions ± 5 kb) to 3′ ends (Sµ regions ± 5 kb) was identified, and their genomic location and CIGAR information were extracted. To counteract the potential PCR bias introduced by the LR-PCR and to account for the presence of the rearranged nonproductive allele in the CH12F3 cell line [15, 23], only unique breakpoints with a ≥10× sequencing depth were used for downstream analysis of repair location and signature. Breakpoints located (5′ and/or 3′ end(s)) outside of either the Sµ or Sα regions were defined as a resected join.

Author Contributions

Ludovic Deriano and Chloé Lescale conceived the study. Ludovic Deriano supervised the work and acquired funding. Chloé Lescale performed experiments and analyzed the data. Guillaume Rode helped with generating knockout B cell clones and with experiments. Timea Marton generated the S8 and S25 B cell clones. E.V. performed CSR assays in CH12F3 cells complemented with SHLD1 mutants. Timea Marton and Amaury Vaysse established the PacBio CSR breakpoint analysis pipeline and analyzed data. François Dossin developed the dual sgRNA-expression plasmid. Alice Libri helped generate the dual sgRNA-expression plasmid and perform germline transcript experiments. Chloé Lescale and Ludovic Deriano wrote the manuscript.

Conflicts of Interest

The authors declare no conflicts of interest.

Data Availability Statement

The long-range PCR sequencing (Pacbio) data have been deposited in NCBI's Sequence Read Archive under the accession number PRJNA1235282. All data are available from the authors upon reasonable request.

References

1. A. Libri, T. Marton, and L. Deriano, "The (Lack of) DNA Double-Strand Break Repair Pathway Choice during V(D)J Recombination," *Frontiers in Genetics* 12, 823943 (2021), https://doi.org/10.3389/fgene.2021.823943.

2. Y. Feng, N. Seija, J. M. Di Noia, and A. Martin, "AID in Antibody Diversification: There and Back Again," *Trends in Immunology* 41 (2020): 586–600, https://doi.org/10.1016/j.it.2020.04.009.

3. J. Chaudhuri and F. W. Alt, "Class-Switch Recombination: Interplay of Transcription, DNA Deamination and DNA Repair," *Nature Reviews Immunology* 4 (2004): 541–552.

4. T. Saha, D. Sundaravinayagam, and M. Di Virgilio, "Charting a DNA Repair Roadmap for Immunoglobulin Class Switch Recombination," *Trends in Biochemical Sciences* 46 (2021): 184–199, https://doi.org/10.1016/j.tibs.2020.10.005.

5. L. Deriano and D. B. Roth, "Modernizing the Nonhomologous End-joining Repertoire: Alternative and Classical NHEJ Share the Stage," *Annual Review of Genetics* 47 (2013): 433–455, https://doi.org/10.1146/annurev-genet-110711-155540.

6. E. Kabrani, T. Saha, and M. Di Virgilio, "DNA Repair and Antibody Diversification: The 53BP1 Paradigm," *Trends in Immunology* 44 (2023): 782–791, https://doi.org/10.1016/j.it.2023.08.004.

7. Z. Mirman and T. de Lange, "53BP1: A DSB Escort," *Genes & development* 34 (2020): 7–23, https://doi.org/10.1101/gad.333237.119.

8. D. Setiaputra and D. Durocher, "Shieldin—The Protector of DNA Ends," *Embo Reports* (2019): 20, https://doi.org/10.15252/embr.201847560.

9. Z. Mirman, S. Cai, and T. de Lange, "CST/Polalpha/Primase-Mediated Fill-in Synthesis at DSBs," *Cell Cycle* 22 (2023): 379–389, https://doi.org/10.1080/15384101.2022.2123886.

10. Z. Mirman, N. K. Sasi, A. King, J. R. Chapman, and T. de Lange, "53BP1-Shieldin-Dependent DSB Processing in BRCA1-Deficient Cells Requires CST-Polalpha-primase Fill-in Synthesis," *Nature Cell Biology* 24 (2022): 51–61, https://doi.org/10.1038/s41556-021-00812-9.

11. J. Paiano, et al., "Role of 53BP1 in End Protection and DNA Synthesis at DNA Breaks," *Genes & Development* 35 (2021): 1356–1367, https://doi.org/10.1101/gad.348667.121.

12. E. Vincendeau, et al., "SHLD1 is Dispensable for 53BP1-dependent V(D)J Recombination but Critical for Productive Class Switch Recombination," *Nature Communications* 13 (2022): 3707, https://doi.org/10.1038/s41467-022-31287-3.

13. A. K. Ling, et al., "SHLD2 promotes Class Switch Recombination by Preventing Inactivating Deletions Within the Igh Locus," *Embo Reports* (2020): e49823, https://doi.org/10.15252/embr.201949823.

14. H. Ghezraoui, et al., "53BP1 cooperation With the REV7-Shieldin Complex Underpins DNA Structure-specific NHEJ," *Nature* (2018), https://doi.org/10.1038/s41586-018-0362-1.

15. M. Nakamura, et al., "High Frequency Class Switching of an IgM+ B Lymphoma Clone CH12F3 to IgA+ Cells," *International Immunology* 8 (1996): 193–201.

16. M. Barazas, et al., "The CST Complex Mediates End Protection at Double-Strand Breaks and Promotes PARP Inhibitor Sensitivity in BRCA1-Deficient Cells," *Cell reports* 23 (2018): 2107–2118, https://doi.org/10.1016/j.celrep.2018.04.046.

17. A. King, et al., "Shieldin and CST Co-Orchestrate DNA Polymerase-Dependent Tailed-end Joining Reactions Independently of 53BP1-Governed Repair Pathway Choice," *Nature Structural & Molecular Biology* (2024), https://doi.org/10.1038/s41594-024-01381-9.

18. R. A. Hom and D. S. Wuttke, "Human CST Prefers G-Rich but Not Necessarily Telomeric Sequences," *Biochemistry* 56 (2017): 4210–4218, https://doi.org/10.1021/acs.biochem.7b00584.

19. P. Gu, et al., "CTC1 deletion Results in Defective Telomere Replication, Leading to Catastrophic Telomere Loss and Stem Cell Exhaustion," *Embo Journal* 31 (2012): 2309–2321, https://doi.org/10.1038/emboj.2012.96.

20. H. Dev, et al., "Shieldin Complex Promotes DNA End-joining and Counters Homologous Recombination in BRCA1-Null Cells," *Nature Cell Biology* 20 (2018): 954–965, https://doi.org/10.1038/s41556-018-0140-1.

21. C. Sifri, L. Hoeg, D. Durocher, and D. Setiaputra, "An AlphaFold2 Map of the 53BP1 Pathway Identifies a Direct SHLD3-RIF1 Interaction Critical for Shieldin Activity," *Embo Reports* 24 (2023): e56834, https://doi.org/10.15252/embr.202356834.

22. S. W. Cai, et al., "POT1 Recruits and Regulates CST-Polalpha/Primase at Human Telomeres," *Cell* 187 (2024): 3638–3651, https://doi.org/10.1016/j.cell.2024.05.002.

23. L. Han, S. Masani, and K. Yu, "Overlapping Activation-induced Cytidine Deaminase Hotspot Motifs in Ig Class-switch Recombination," *PNAS* 108 (2011): 11584–11589, https://doi.org/10.1073/pnas.1018726108.

24. X. Zhang, et al., "Fundamental Roles of Chromatin Loop Extrusion in Antibody Class Switching," *Nature* 575 (2019): 385–389, https://doi.org/10.1038/s41586-019-1723-0.

25. A. M. Refaat, et al., "HNRNPU Facilitates Antibody Class-Switch Recombination Through C-NHEJ Promotion and R-Loop Suppression," *Cell reports* 42 (2023): 112284, https://doi.org/10.1016/j.celrep.2023.112284.

26. C. Boboila, et al., "Alternative End-Joining Catalyzes Robust IgH Locus Deletions and Translocations in the Combined Absence of Ligase 4 and Ku70," *PNAS* 107 (2010): 3034–3039, https://doi:0915067107.

27. C. T. Yan, et al., "IgH Class Switching and Translocations Use a Robust Non-Classical End-Joining Pathway," *Nature* 449 (2007): 478–482, https://doi.org/10.1038/10.1038/nature06020.

28. C. Madru, et al., "DNA-binding Mechanism and Evolution of Replication Protein A," *Nature Communications* 14 (2023): 2326, https://doi.org/10.1038/s41467-023-38048-w.

29. C. J. Lim, et al., "The Structure of Human CST Reveals a Decameric Assembly Bound to Telomeric DNA," *Science* 368 (2020): 1081–1085, https://doi.org/10.1126/science.aaz9649.

30. A. B. Hayran, et al., "RPA Guides UNG to Uracil in ssDNA to Facilitate Antibody Class Switching and Repair of Mutagenic Uracil at the Replication Fork," *Nucleic Acids Res.* 52 (2024): 784–800, https://doi.org/10.1093/nar/gkad1115.

31. J. Chaudhuri, C. Khuong, and F. W. Alt, "Replication Protein A Interacts With AID to Promote Deamination of Somatic Hypermutation Targets," *Nature* 430 (2004): 992–998.

32. M. Zhang, et al., "Mammalian CST Averts Replication Failure by Preventing G-quadruplex Accumulation," *Nucleic Acids Res.* 47 (2019): 5243–5259, https://doi.org/10.1093/nar/gkz264.

33. Q. Qiao, et al., "AID Recognizes Structured DNA for Class Switch Recombination," *Molecular Cell* 67 (2017): 361–373, https://doi.org/10.1016/j.molcel.2017.06.034.

34. M. Rogier, et al., "Fam72a Enforces Error-Prone DNA Repair During Antibody Diversification," *Nature* 600 (2021): 329–333, https://doi.org/10.1038/s41586-021-04093-y.

35. C. Lescale, et al., "RAG2 and XLF/Cernunnos Interplay Reveals a Novel Role for the RAG Complex in DNA Repair," *Nature Communications* 7, 10529 (2016), https://doi.org/10.1038/ncomms10529.

Supporting Information

Additional supporting information can be found online in the Supporting Information section.